

**Liquid Fuels: Pyrolytic Degradation and Fire Spread Behavior as Influenced by
Buoyancy**

Final Technical Report

For

NASA Grant No: NCC3-707

Submitted to

National Aeronautics and Space Administration
Attn: Dr. Howard D. Ross (Program Manager)
Glenn Research Center
Cleveland, OH 44135-1062

By

Professor Yaw D. Yeboah
Combustion and Emission Control Lab
Department of Engineering
Clark Atlanta University
Atlanta, GA 30314

June 2003

TABLE OF CONTENTS

ABSTRACT.....	2
1. INTRODUCTION AND OBJECTIVES.....	4
2. EXPERIMENTAL APPARATUS.....	8
3. RESULTS AND DISCUSSION.....	16
3.1 Observation of flame spread with HSVS.....	16
3.2 Flame spread analysis with PIV.....	18
3.3 Flame spread analysis with LDV.....	29
3.4 Candle flame analysis with LDV.....	35
4. SUMMARY AND CONCLUSIONS.....	44
5. RECOMMENDATIONS.....	47
6. REFERENCES.....	48

ABSTRACT

This project was conducted by the Combustion and Emission Control Lab in the Engineering Department at Clark Atlanta University under NASA Grant No. NCC3-707. The work aimed at providing data to supplement the ongoing NASA research activities on flame spread across liquid pools by providing flow visualization and velocity measurements especially in the gas phase and gas-liquid interface.

During this investigation, the detailed physics of flame spread across liquid pools was revealed using particle image velocimetry (PIV), 3-dimensional laser Doppler velocimetry (LDV) and high-speed video imaging system (HSVS). Flow fields (front and side views) of both the liquid and gas phases were visually investigated for the three subflash regimes of flame spread behavior.

Some interesting findings obtained from the front and side views on flame spread across butanol pools are presented. PIV results showed the size of the transient vortex in the liquid phase near the flame front varied with the initial pool temperature. The transient vortex ahead of the flame front in the gas phase was, for the first time, clearly observed located just within 0-3 mm above the liquid surface and its size was dependent on the initial pool temperature. We calculated the flow velocity at 1 mm below the liquid surface near the flame front and inferred the generation mechanism of the vortex in the gas phase. Finally, after comparison of the flow velocity of the liquid surface and the flame spread rate, a reasonable explanation to the formation mechanism of the pulsating characteristic was proposed. This explanation is compatible with the previous numerical calculations and deductions.

In the gas phase, two recirculation cells with size of the order of 5-10 millimeters in the plane perpendicular and against the flame spread direction (side view) were observed ahead of the flame front. The side view also revealed how they were broken as the flame front approached. The effect of thermal expansion in the gas phase near the flame front is believed to be the dominant factor in the destruction of the cell.

Measurements of the flow structure of the flame spread were also conducted using LDV system. The LDV results were consistent with the results from the PIV and high-speed imager.

To investigate the flow pattern and the buoyancy influence of a candle flame, LDV measurements around a candle flame were also conducted. At the nearby region (within 20 mm radius from the flame center), the direction of radial components was always toward the candle center and the direction of axial components was upwards. The radial component did not change significantly. However, the upward velocity component dramatically changed. The closer the flame was to the measurement position, the faster the upward velocity component increased.

1. INTRODUCTION AND OBJECTIVES

Flame spread across liquid fuel pools is of special interest due to increased practical concerns of fire safety and the complexity of the phenomena among research groups. Scientific research in this area was first reported in the 1930s[1] and flourished between 1955 to 1980. In 1981, Glassman and Dryer provided a summary of the work to that time [2]. Newer studies including experimental and numerical progress were summarized in 1994 by Ross [3]. There are still many remaining questions that need to be investigated clearly (e.g., buoyancy effects and pulsating mechanism).

The role of buoyancy-related processes regarding the mechanisms of flame spread is an area of research that needs further attention. Buoyancy forces can affect the liquid-phase convective fields and consequently the rate of liquid preheating, the fuel-air mixing, and the rate of chemical reaction [4]. Gas-phase buoyant flow transports oxidizer to the flame zone and hot products away from the zone. Liquid-phase convection, due to both thermocapillarity and buoyancy, transports heated liquid ahead of the leading edge of the flame.

There have been several attempts involving particle image velocimetry (PIV), rainbow schlieren deflectometry (RSD), standard schlieren deflectometry (SSD), infrared thermography (IT), holographic interferometry (HI) and laser Doppler velocimetry (LDV) to determine flow patterns and velocities in the liquid phase, but earlier effort did not use the same technique for all flame spread regimes. Often RSD, IT, SSD and HI were used for qualitative purposes, in which a qualitative thermal field image was used to infer the flow field. Previous investigators have pointed out the uncertainty in the use of thermal fields to infer velocity fields.

In the uniform spread regime, HI was used to imply that liquid-phase convection controls the uniform spread rate for very narrow pools, e.g. for 0.5 cm wide pools [5]. In wider pools, Miller and Ross [6] observed through PIV that liquid convection is confined to a very thin, surface layer and, since the flame overtakes it, convection cannot be the only preheating mechanism (in flame-fixed coordinates, the flow is toward the flame).

Newman [7] used LDV to measure the gas-phase velocities above a liquid pool as a flame passed. This technique was difficult to apply to an unsteady phenomenon, and more importantly, the apparatus prohibited measurements any lower than 2 mm above the liquid pool surface. From his data, no recirculation cell of the predicted type could be inferred. Additional research by Newman reported in Santoro et al [8] provides a time-lapse photograph with 3 particle streaklines descending toward the fuel surface just ahead of the flame. These streaklines change direction as they approach the liquid; when combined with other particle streaklines and the LDV measurements farther above the pool, they show a flow reversal that didn't necessarily prove the existence of a gas-phase recirculation cell.

In the pseudo-uniform regime, SSD has been used to view the size of the heated vortex ahead of and under the flame [9]. The authors reported that the vortex reached the size of their tray (40 cm long x 4 cm deep) and felt that the presence of the end wall was affecting their results. In contrast to experiments, modeling of the problem has elucidated the existence and importance of the cell. Furuta et al [10] examined mixed convective airflow during flame spread over a shallow fuel layer in the pseudo-uniform flame spread regime. As hypothesized by Sirignano [11], Furuta et al [10] showed that thermal expansion accompanying combustion has an overwhelming effect on the gas-phase flow

field in the very near vicinity of the flame, and quantified the coupling of the gas-phase and liquid-phase processes.

The gas-phase flow field has been visualized by releasing smoke traces [12] or small particles into the gas [13]. One experimental difference between these techniques has been noted: with the smoke tests, a fan imposed an opposed airflow that maintained the smoke on streamlines parallel to the fuel surface as the flame approached. The smoke was observed to curl around and form the recirculation cell. In the gas PIV experiments, small particles were placed in the air and gradually settled vertically toward the surface, the airflow in this case was buoyantly driven, and the recirculation cell was not observed to form as fully as with an imposed airflow. Smoke-flow tests without an imposed flow also have not previously revealed a full recirculation cell, but did clearly show airflow toward the flame.

Shiller et al. [14], developed a numerical model with kinetics and variable thermophysical properties in both the gas and liquid phases. They concluded that pulsation owes its existence to the gas-phase circulation cell, and thermal expansion plays the major role in the periodic destruction of the circulation cell in the gas phase when the flame jumps forward during the pulsating spread. Its formation occurs during the crawling portion of the pulsating flame cycle, and it persists in accumulating fuel vapor until a flammable concentration is attained inside the cell and the flame jumps again.

This study was undertaken to support the ongoing research activities at NASA on flame spread across liquid pools. The objectives of the project were to:

- Design, construct and test an experimental system to study flame spread behavior in liquid pools in normal gravity conditions.
- Confirm experimentally the existence of the vortex in the gas phase ahead of the flame front.
- Provide insights into the flow structure during flame spread in all sub-flash regimes of flame spread behavior, and
- Compare the results of the particle image velocimetry, laser Doppler velocimetry and high speed video imaging studies.

This final report on NASA Grant No: NCC3-707 reflects the results of the activities conducted during the project from March 1999 to March 2003.

2. EXPERIMENTAL APPARATUS

The major components of the experimental setup and instrumentation for the project included a tray of liquid pool, ignitor, temperature measurement system, imaging or High Speed Video System (HSVS), Particle Image Velocimetry (PIV) and Laser Doppler Velocimetry (LDV) systems. Figure 2.1 is the schematic of the experimental setup. The major components of the experimental setup and instrumentation are described below.

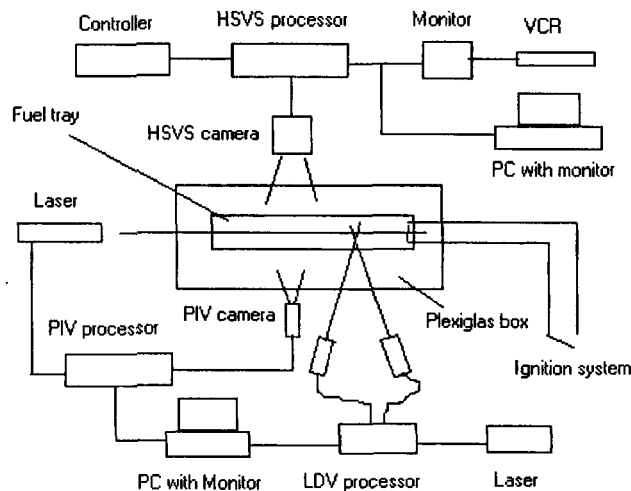


Figure 2.1 The schematic of the experimental setup

2.1 Fuel Tray

The tray provided by NASA had inside dimensions of 30 cm long, 2 cm wide and 2 cm deep and its bottom had cooling chambers to control the fuel initial temperature, which has been found to have a significant effect on the characteristics of the flame spread. This tray was modified for flow visualization and velocity measurements. A slit about 4 mm wide was cut at one end of the tray for the laser path to

enable the use of the laser diagnostics. The use of this tray that had previously been used for experiments at NASA enabled comparisons and generalizations of the results of this study with those obtained at NASA.

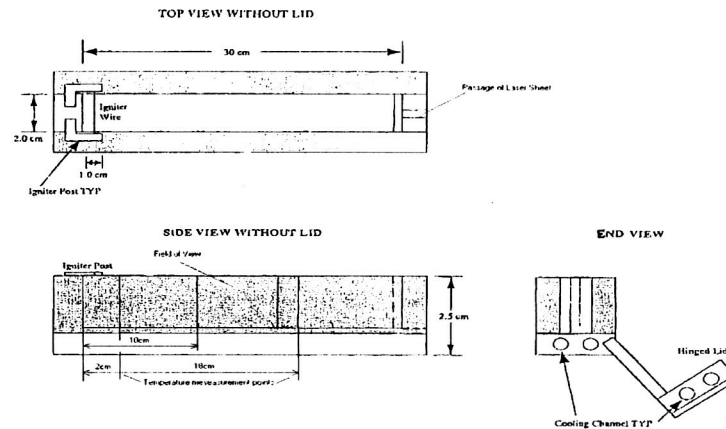


Figure 2.2. The schematic of the modified tray

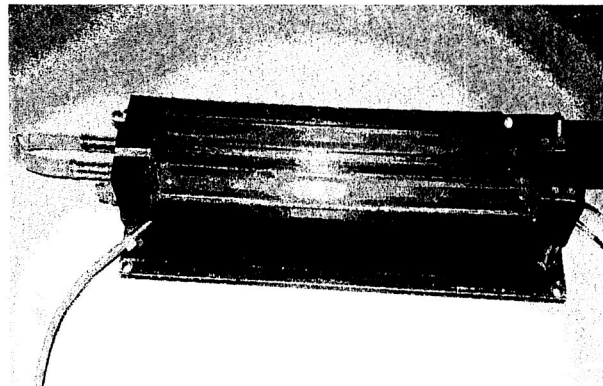


Figure 2.3 Photograph of the modified fuel tray provided by NASA

Figure 2.2 is the schematic of the modified tray. The field of view is defined by the area, which the camera focuses on. The laser generated by a pulse laser (532 nm YAG laser) passed through the slit of the tray (see Figure 2.1). Figure 2.3 is a photograph of the modified NASA tray.

2.2 Ignition System

An igniter wire was installed at one end of the tray of liquid pool. Thus, the liquid fuel was ignited at one end and the flame propagated to the other end of the tray. The ignition was accomplished with electrical power controlled by a 10 amp variable transformer. The experiments were performed with the tray in a transparent Plexiglas box with dimensions of 61 cm \times 61 cm \times 46 cm. All openings of the Plexiglas box were closed to ensure a quiescent environment. A HP thermal meter was used to measure the initial temperature of the fuel pool.

2.3 Smoke generator

Figure 2.4 shows a picture of the smoke generator designed, constructed and used in the studies.

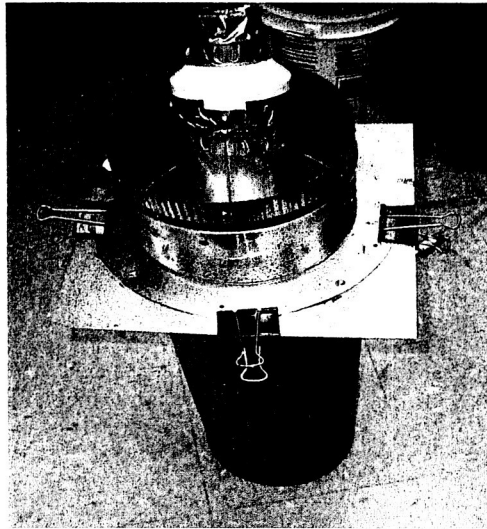


Figure 2.4 Smoke generator

The smoke generator provided seeding particles for the PIV and LDV measurements of the gas phase. The soot particle size was estimated to be of the order of 1-2 microns.

Aluminum oxide was used as the seeding particle for the liquid (fuel) phase. The particle size of the aluminum oxide was between 1~10 micron meters.

2.4 Particle Image Velocimetry (PIV)

A Dantec Flow Map PIV 400 system was used for flow velocity field measurements of the gas and liquid phases. The PIV system included:

- A 15 Hz dual cavity Nd:YAG laser with power up to 400 mJ/p at wavelength 532 nm.
- A Kodak 700 double image CCD camera.
- A 2000 PIV processor to coordinate camera and laser actions.
- Flow Manager 3.12 Software for data collection and processing.

Figure 2.5 shows a picture of the experimental setup with the PIV system.

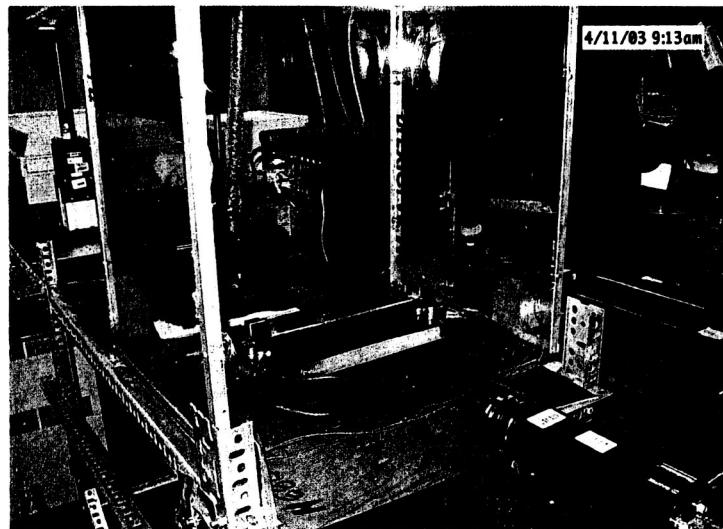


Figure 2.5 Photograph of experimental setup with the PIV system

2.5 Laser Doppler Velocimetry (LDV)

A TSI 9271 laser Doppler velocimeter was set up for 3-dimensional flow velocity field measurements of the gas and liquid phases. The LDV system included the following components:

- An Innova 90 series 5 W Ion laser to provide a multicolored laser beam.
- A model 9201 ColorBurst multicolor beam separator to convert the input beam from the laser into three pairs of beams.
- A model 9800 series two component fiber-optic probe to form a measurement volume.
- A model 9230 ColorLink Plus multicolor receiver to provide frequency shifting.
- Model IFA 755 digital burst correlator to process Doppler frequency information and transmit it to the software.
- A Flow Information Display (FIND) software for windows to analyze the incoming data and provide statistical data analysis and display.

Figure 2.6 shows the experimental setup with the LDV system.

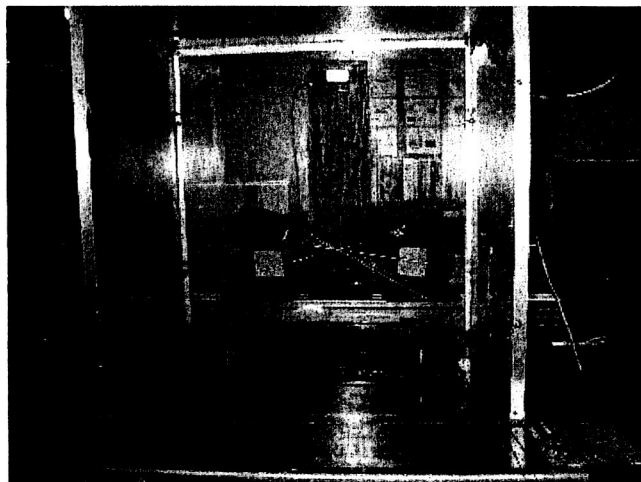


Figure 2.6 Photograph of experimental setup with the LDV system

Figure 2.7 is the non-orthogonal to orthogonal conversion of the three-component measurements of LDV system. In a two-probe, three-component measurement, the most common situation corresponds to two components of velocity being measured using a non-orthogonal system and the third (orthogonal) velocity component being measured directly. In Figure 2.7, the two blue beams in probe 1 that measure the velocity U_b and the two violet beams in the probe 2 that measure the velocity U_v are in the plane of the paper. The third velocity component U_g is perpendicular to the plane of the paper and is measured directly by the two green beams in the plane perpendicular to the paper. U_g is considered to be positive in the direction out of the plane of the paper.

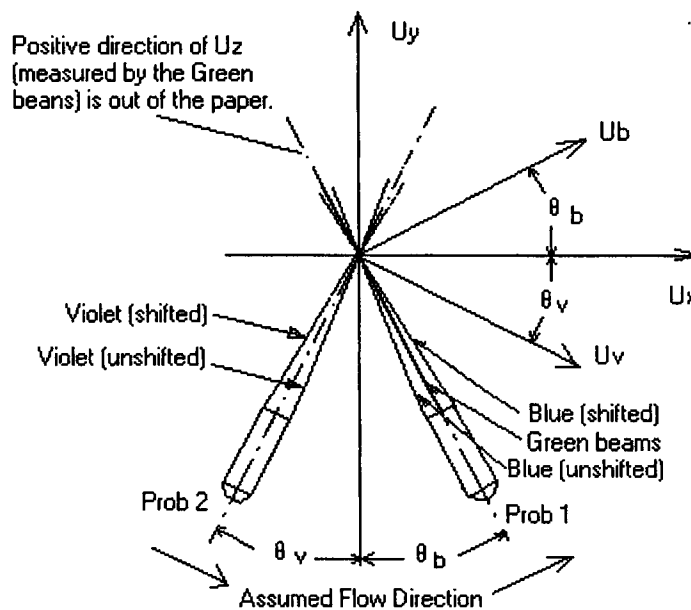


Figure 2.7 Three-Component Measurements of LDA system

The two velocity components U_b and U_v are measured in the U_x - U_y planes. U_g in this study is the same as U_z . The measured non-orthogonal velocity values can be

transformed into the orthogonal coordinate system, where the positive U_z axis is out of the plane of the paper and U_x and U_y directions are as shown in Figure 2.7. U_b and U_v are transformed into U_x and U_y using the following conversion equations.

$$\begin{bmatrix} U_x \\ U_y \\ U_z \end{bmatrix} = \begin{bmatrix} a & b & 0 \\ c & d & 0 \\ 0 & 0 & 1 \end{bmatrix} \begin{bmatrix} U_b \\ U_v \\ U_g \end{bmatrix} = \begin{bmatrix} 0 & a & b \\ 0 & c & d \\ 1 & 0 & 0 \end{bmatrix} \begin{bmatrix} U_g \\ U_b \\ U_v \end{bmatrix}$$

where,

$$a = \frac{\sin \theta_v}{\sin(\theta_b + \theta_v)}$$

$$b = \frac{\sin \theta_b}{\sin(\theta_b + \theta_v)}$$

$$c = \frac{\cos \theta_v}{\sin(\theta_b + \theta_v)}$$

$$d = \frac{-\cos \theta_b}{\sin(\theta_b + \theta_v)}$$

If $\theta_b = \theta_v = 20^\circ$, then

$$\begin{bmatrix} U_x \\ U_y \\ U_z \end{bmatrix} = \begin{bmatrix} 0 & \frac{1}{2 \cos 20^\circ} & \frac{1}{2 \cos 20^\circ} \\ 0 & \frac{1}{2 \sin 20^\circ} & \frac{-1}{2 \sin 20^\circ} \\ 1 & 0 & 0 \end{bmatrix} \begin{bmatrix} U_b \\ U_v \\ U_g \end{bmatrix}$$

In the experiments, the angles between probe 1 and the centerline (θ_b) as well as probe 2 and the centerline (θ_v) were fixed at 20° .

2.6 High Speed Video Imager System

A Kodak EktaPro high-speed intensified imager with controller and a Nikon micro lens attached to a charge coupled device (CCD) camera were used to study the flame propagation. Specification for the camera system include a frame rate of 30-12,000 fps, sensitivity of more than 50% peak from 440 nm to 700 nm, and a variable grab time from 10-5000 ns. Output from the imager system was recorded on a video recorder or a computer.

Figure 2.8 is a photograph of the high-speed video imager system (HSVS)



Figure 2.8 Photograph of HSVS system

3. RESULTS AND DISCUSSION

Flame spread observations were carried out at initial pool temperatures from 18°C to 40 °C using butanol as fuel. The flame spread behavior was observed by the high-speed imager, the PIV and LDV systems.

The three regimes of flame spread behavior and the pulsating character of the flame front were clearly revealed by the images. The flow structures of the liquid and gas phases were analyzed by the PIV through different visual directions (front view, side view and top view). The flow near the flame spread front was also measured by 3-D LDV system to confirm the PIV measured results.

Most experiments were repeated at least three times (generally 3-5 times). The experimental measurements and flame spread behavior were repeatable based on image comparisons and standard error calculations.

3.1 Observation of flame spread with high speed imager

Figure 3.1 shows the experimental results of flame spread rate versus initial pool temperature using butanol as fuel. The magnitude of the flame spread rate, V_f is a strong function of initial pool temperature T_0 . Three distinct regimes of flame spread slopes can be observed from Figure 3.1: the pseudo-uniform regime (below 20°C), uniform regime (above 31°C) and pulsating regime (from 22°C to 30°C). In the pulsating regime, the flame spread pulsates as it propagates. The flame spread rates shown in Figure 3.1 for this regime are mean values.

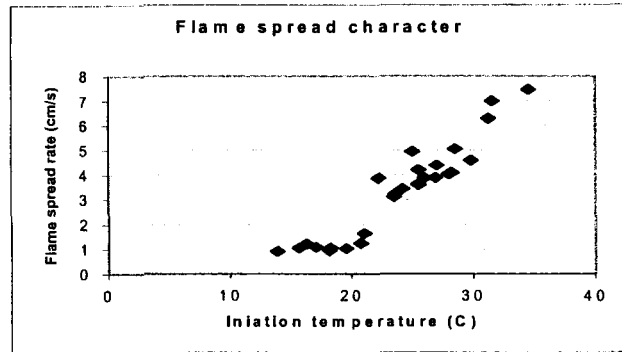


Figure 3.1 Flame spread characteristic regimes of butanol

The flame front position with time as a function of initial pool temperature is illustrated in Figure 3.2. The rate (mean value) of the flame spread showed a strong dependence on initial pool temperature. Three regimes of flame spread behavior are revealed in Figure 3.2. In the pulsating regime, the jump velocity (positive slopes between jumps) appears to be independent of initial pool temperature. However the crawl velocity (descending slopes between jumps) is clearly dependent on the initial temperature. The backward spread or crawl velocity decreased as the initial pool temperature increased.

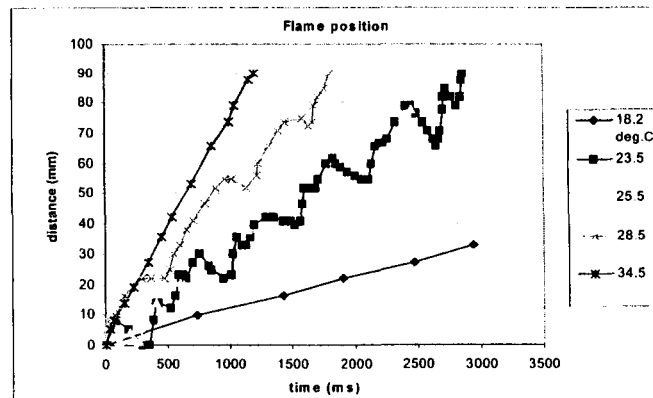


Figure 3.2 Flame position vs. time for different initial pool temperatures

An interesting phenomenon observed in the visualization study was that the flame retreats before it surges forward with increasing brightness. Besides the pulsation behavior of the flame front, in the pulsating regime, pulsations behind the flame front were also observed. Figure 3.3 is a recorded image of the phenomenon at the initial pool temperature of 25.5 °C. In the area behind the flame front and at the liquid-flame interface, pulsation occurred two or three times during a single flame front pulsating period.

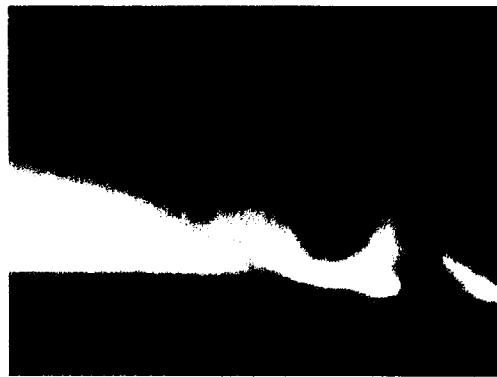


Figure 3.3 Observation of pulsating flame spread with high speed imager

3.2 Flame spread analysis with PIV

The camera with a micro lens was used to enlarge the target area. The camera view area was approximate 16 mm long \times 12 mm wide. The flow and flame structures near the flame front were clearly revealed with the enlarged target area. The velocity vector field of flow pattern in the liquid phase was obtained by PIV. The flow and flame structures in the gas phase were analyzed through PIV images and not the vector fields. It was difficult to obtain clear and accurate flow vector fields near the flame due to seeding and illumination problems.

3.2.1 Results from front view

The gas phase fields were analyzed at different initial pool temperatures from 18°C to 40°C. Figure 3.4 shows the transient recirculation cell in the gas phase visualized by PIV system. All PIV images (including Figure 3.4 and Figure 3.5) were obtained in the plane along the propagation direction and perpendicular to the liquid surface. Figure 3.4 is the spread behavior of the transient recirculation cell in the gas phase at an initial pool temperature of 20°C. This flame spread behavior falls in the pseudo-uniform region. The PIV images were taken as the recirculation cell propagated through the camera view area. Figure 3.4 clearly shows the size and relative position of the vortex in the gas phase. The vortex was approximately 12 mm long and 1 mm high. It was located right ahead of the flame front and above the liquid surface.

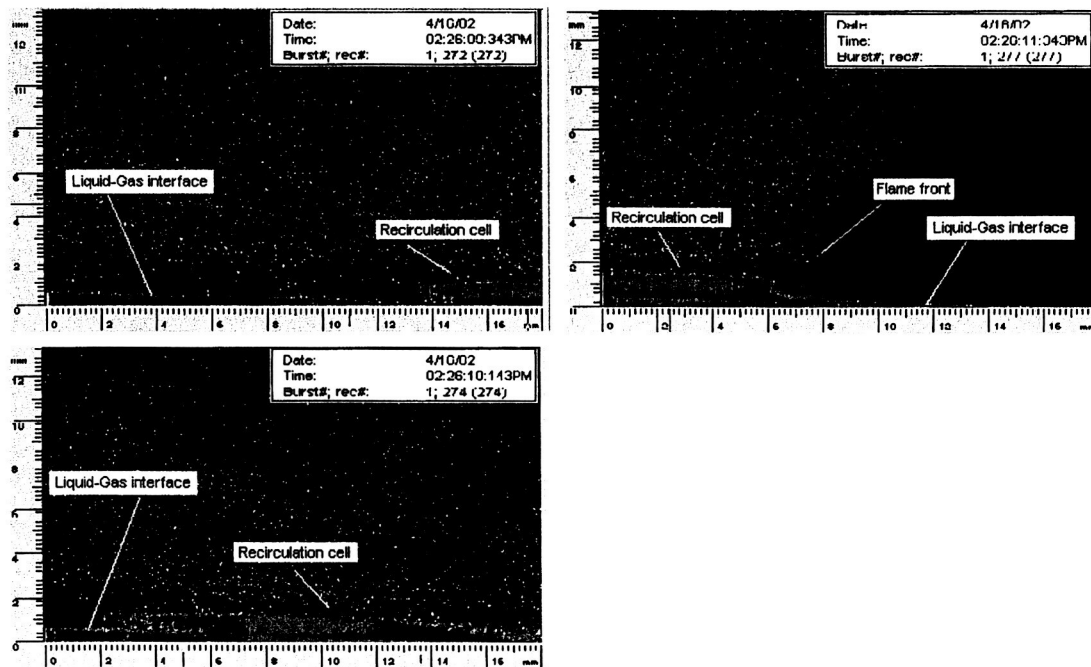


Figure 3.4 The spread behavior of recirculation cell at initial pool temperature of 20°C

Figure 3.5 was acquired in the gas phase at 18° C, 20°C, 22°C and 26°C, respectively. The height of the vortex with initial pool temperature of 18°C was 2.8 mm

and it was 1.0 mm and 0.8 mm for vortices with initial pool temperatures of 20°C and 22°C, respectively. We did not find a detectable size vortex in the gas phase near the flame front for the cases with initial pool temperatures more than 24°C, including 26°C shown in Figure 3.5. These images indicate that the size of the vortex ahead of the flame front in the gas phase decreased as the initial temperature increased.

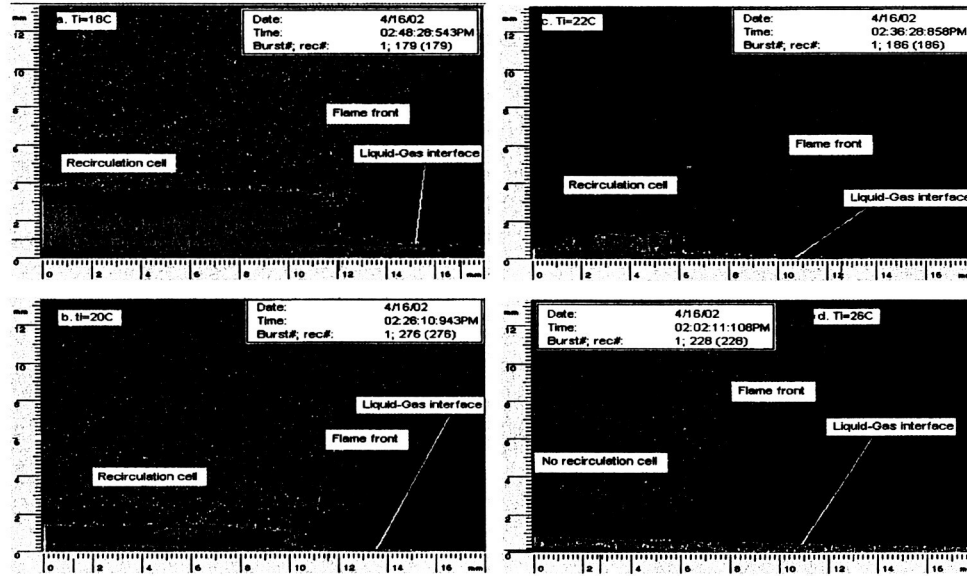


Figure 3.5 The comparison of the vortex in the gas phase obtained at different initial pool temperatures

Liquid velocity vector distributions in the plane along the propagation direction and perpendicular to the liquid surface were also obtained at different initial pool temperatures as the flame front propagated through the camera view area.

Figures 3.6 shows the liquid vector distributions before, during and after the flame front passed through the view area of the camera. The initial temperature for these vector fields was 21°C. Figure 3.6 (a) shows that before the flame front reached the camera's object view (i.e., area ahead of the flame front), the flow in the liquid was laminar. As the

flame front passed the view area, some turbulence or recirculation cell (vortex) was observed. The flame front was right above the recirculation cell (Figure 3.6 (b)). The velocity field returned to laminar after the passage of the flame front with only very slight recirculation (Figure 3.6 (c)).

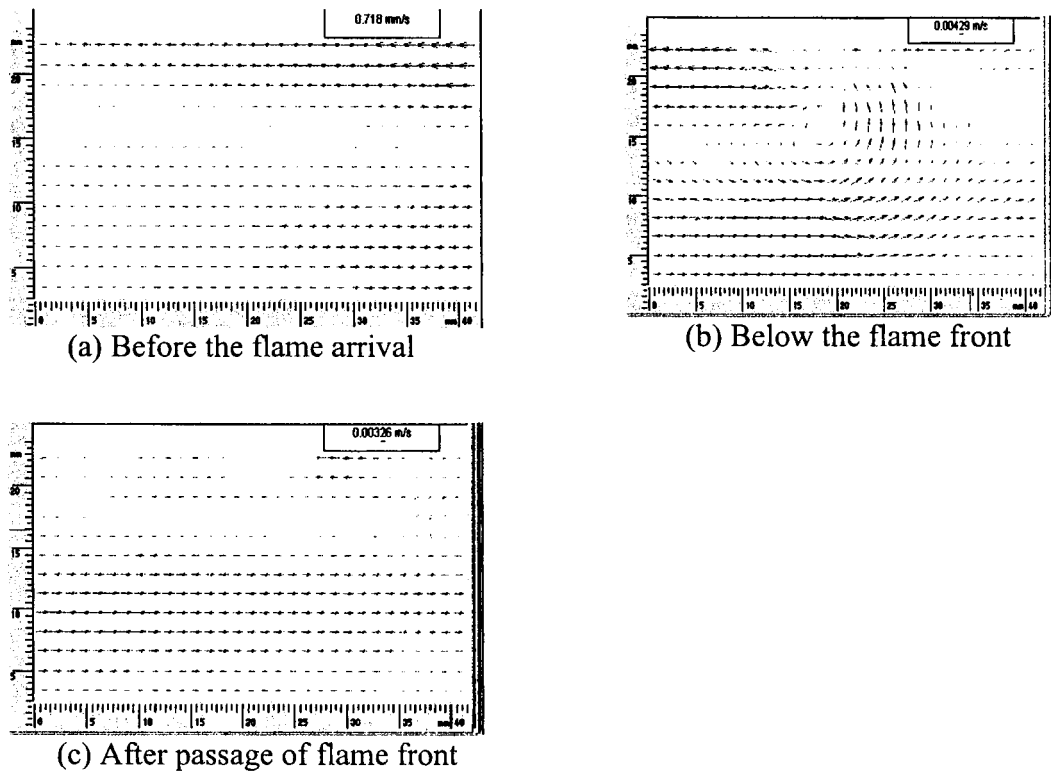


Figure 3.6 Liquid vector fields below the flame front with initial pool temperature of 21°C

Shown in Figure 3.7 are the liquid velocity vector fields at initial pool temperatures of 18°C, 23°C and 33°C, respectively. At 18°C, the boundary of the vortex almost reached the bottom of the pool. In contrast, the vortices were much smaller at 23°C and 33°C. Thus, Figure 3.7 indicates that the size of the vortex below the flame

front decreased as the initial pool temperature increased. The experiments also showed that the velocity field returned to laminar after the passage of the flame front with little or no vortex as indicated earlier.

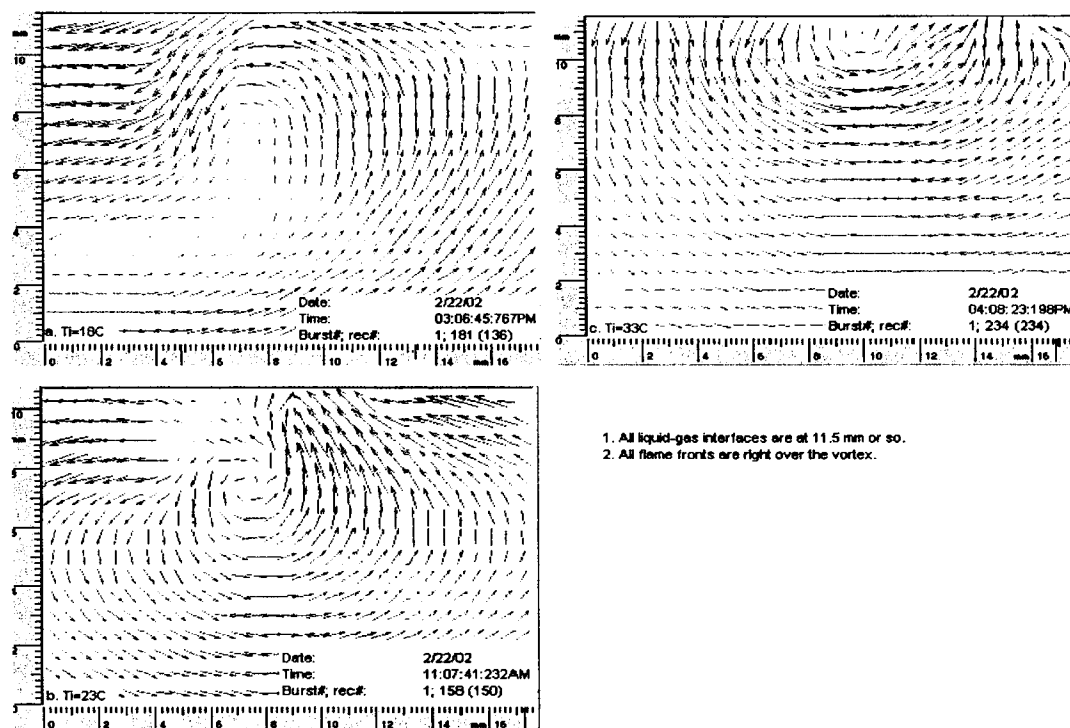


Figure 3.7 The comparison of vortex in the liquid phase at different initial temperatures

According to Figures 3.5 and 3.7, the vortex in the liquid phase showed similar characteristics as in the gas phase, i.e., all vortices in both gas and liquid phases were transient and the size of the vortex decreased as the initial pool temperature increased.

Figure 3.8 gives the liquid phase mean velocity comparison at different initial pool temperatures. Each velocity was calculated as the mean velocity within a strip area with 1 mm width, the camera view as length and located within 1 mm below the liquid surface during the period that the flame front passed the camera view area. The velocity at 1 mm below the liquid surface was chosen because it was hard to obtain the velocity vectors close to the liquid surface due to seeding and illumination problems. The figure

shows that the mean velocity was significantly increased near the flame front at all initial pool temperatures as the flame front passed the view area. After the flame front passed the view area, the velocities in the liquid phase returned closer to their previous values. In addition, the higher the initial pool temperature, the smaller the peak mean velocity obtained. This observation may be the result of the contributions from convection, thermal gradient and flame spread rate.

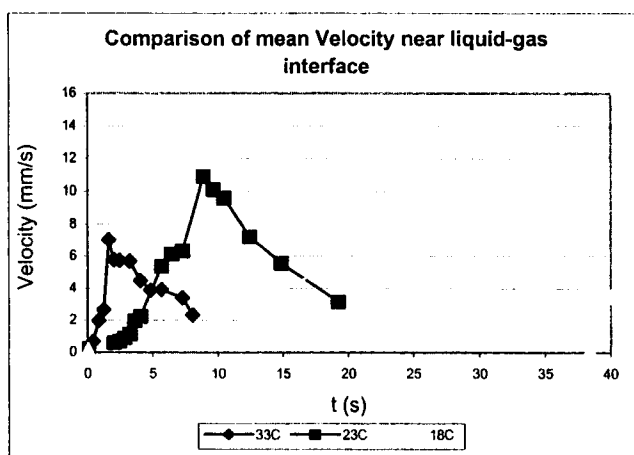


Figure 3.8 Comparison of mean velocity near liquid-gas interface

The flame spread rate and the flow velocity at the liquid-gas interface were calculated and are shown in Figure 3.9. The flow rates at 1 mm below the interface and the flame spread velocities are directly from Figures 3.2 and Figure 3.8. The flame spread rates are the average values at each initial pool temperature. The flow velocities are the peak values in Figure 3.8. The flow velocity at the interface is expected to be higher than the flow velocity at 1 mm below the interface. For the convenience of qualitative discussion, however, we used 1.5 times the flow velocity at 1 mm below the interface as the velocity at the interface. Figure 3.9 indicates that the flame spread rate is less than

the interface flow velocity in the pseudo-uniform, may be less or more in the pulsating regime and is always larger than the interface flow velocity in the uniform regimes.

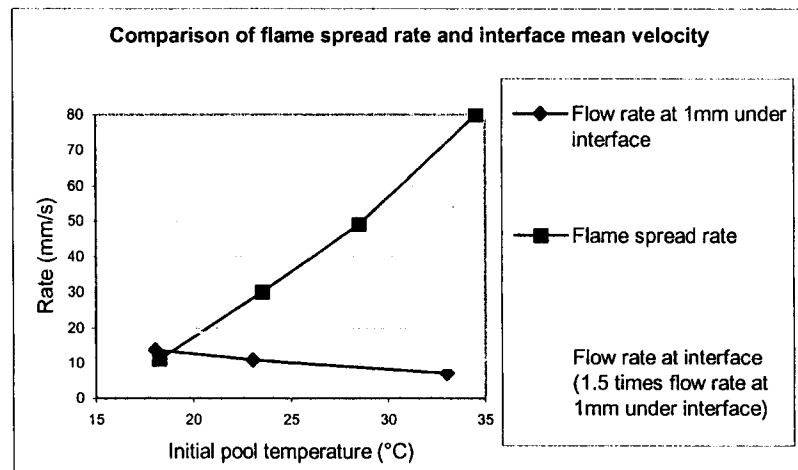


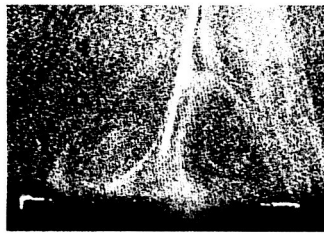
Figure 3.9 Comparison of the flame spread rate and interface mean velocity

3.2.2 Results of gas phase from side view

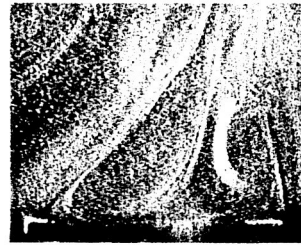
Figure 3.10 shows successive photographs of the gas phase flow field observed in the illumination plane defined by the direction against the flame propagation and perpendicular to the liquid surface.

Two vortices existed until the flame front reached the illumination plane (see Figure 3.10 (a)). These two vortices formed a triangular zone where the fuel and air are presumed well mixed. The triangular premixed zone was believed to have affected and defined the shape and propagation characteristics of the flame. As the flame front reached the illumination plane, the triangular zone with two vortices began to break or disappear due to combustion of the pre-mixed fuel-air ahead of the flame front (see Figure 3.10 (b)). The air flow close to and around the nose of the flame front was in the outward direction due to thermal expansion, emissions of combustion products and the

motion of the flame front. Around the body of the flame front, however, the air flow was into the flame.



(a)



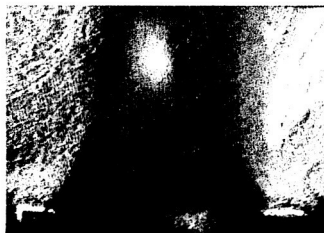
(b)



(c)



(d)



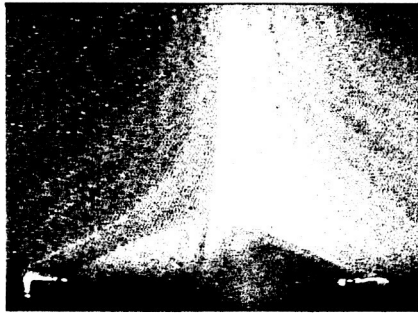
(e)



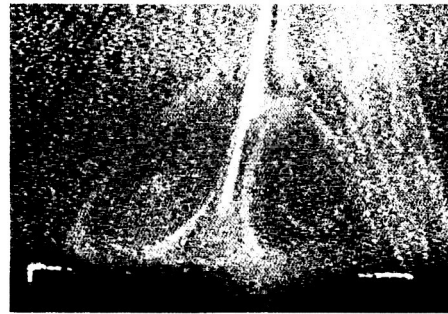
(f)

Figure 3.10 The gas phase velocity fields side view of flame spread at initial pool temperature of 28°C

Figure 3.11 shows comparison of the pre-mixing recirculation cells with initial pool temperatures of 21°C and 28°C. The higher the initial temperature, the larger the two recirculation cells and the triangular premixed zone area. Increased gasification rate of the fuel and buoyancy at higher temperatures are believed to contribute to this phenomenon.



(a) 21°C



(b) 28°C

Figure 3.11 The comparison of flame spread with different initial pool temperatures

3.2.3 Discussion on the experimental results with PIV

Figure 3.12 is a schematic representation of the general flow structure in the gas and liquid phases near the flame front.

The general flow direction near the top of the liquid phase is from right to left. Near the bottom of the pool the liquid flow direction is reversed. The flow velocity reached its maximum right below the flame front and then sharply reduced (see Figure 3.7). There was one vortex observed with counterclockwise movement near the flame front in the liquid.

The general flow direction in the gas phase far above the liquid-gas interface (3 mm or more) and ahead of the flame front was from left to right (i.e., the reverse direction of the flame front). Just right above the liquid-gas interface (0-3 mm) and ahead of the flame, the flow was laminar as expressed in the schematic. In addition, a small vortex right ahead of the flame front could be observed at initial pool temperatures 20°C or lower in the gas phase. It sometimes could be obtained between 22°C and 24°C, and was never observed at initial pool temperatures 26°C or more.

As indicated earlier, when viewed against the flame propagation and perpendicular to the liquid surface, Section A-A in the Figure 3.12, there were two vortices, which formed a triangular zone where the fuel and air are presumed well mixed far ahead of the flame front. These vortices were not broken until the flame front reached the premixed gas.

The flow structure ahead of the flame front for both gas and liquid phases is illustrated schematically in Figure 3.12.

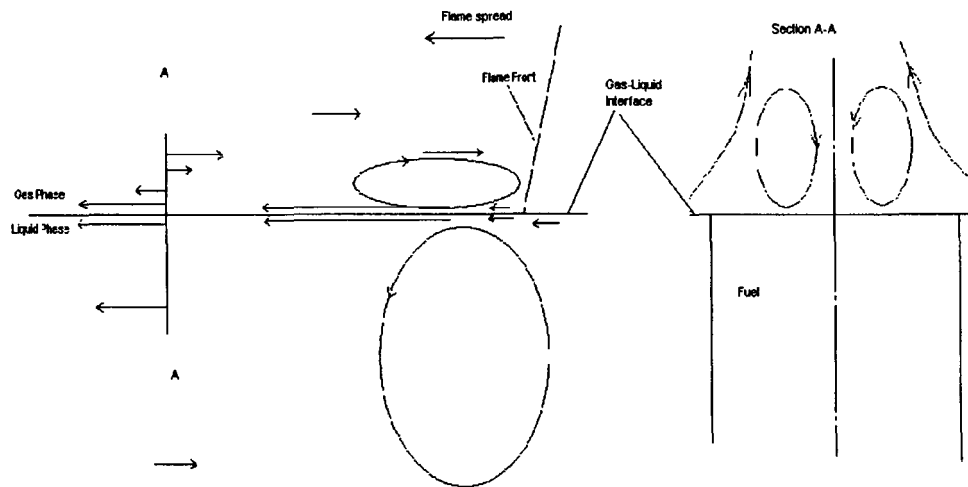


Figure 3.12 The schematic of flame spread near the flame front

Vortices were found in all three flame spread regimes in the liquid phase. However, they were not observed in the gas phase at initial temperatures higher than 26°C. This could be due to limits in the detect ability of the vortex size

The initial pool temperature determined the size of vortices both in the gas and liquid phases. The decrease of vortex size with temperature in the liquid phase is primarily a function of convection and thermal gradient. The decrease in the gas phase, however, is related to the increased gasification, combustion and propagation rate.

No obvious and direct correlation could be drawn between the vortex in the gas phase and the pulsating character of the flame spread because vortices were found in the temperature range 18-26°C which covered the pseudo-uniform regime and the pulsating regime. From Figure 3.9, we can infer that below 20°C (i.e. the pseudo-uniform regime) the interface flow rate is faster than the flame spread rate. In the temperature range of 20-30°C, the flame spread may or may not be faster than the interface flow. Above 30°C, however, the flame spread rate is significantly higher than the interface velocity. Thus, thermal expansion that destroys the gas phase circulation cell and changes in the relative magnitudes of the interface flow velocity and flame spread rate may account for the observed pulsating behavior.

According to the test results from the side view, the higher the initial pool temperature, the more gasified fuel and the larger the two recirculation cells and the triangular premixed zone.

Shiller et al, [14] predicted the existence of a vortex near the interface in the gas phase and concluded that pulsation owes its existence to the gas-phase circulation cell and the thermal expansion plays the major role in the periodic destruction of the circulation cell in the gas phase during the pulsating spread. Compared to this numerical analysis, the experimental results of this study appear to be consistent with their prediction.

3.3 LDV Flame Spread Analysis

3.3.1 Experimental setup

The major components of the experimental setup and instrumentation for the LDV experiments included a fuel tray with inside pool dimension of $30\text{ cm} \times 2\text{ cm} \times 2\text{ cm}$, a Laser Doppler Velocimetry (LDV) system, a transparent Plexiglas box with dimensions of $61\text{ cm} \times 61\text{ cm} \times 46\text{ cm}$, and an experimental table. Propanol was used as fuel in the LDV measurements.

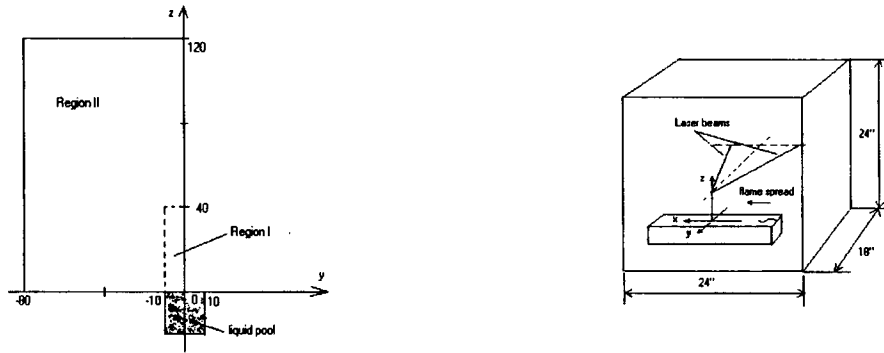


Figure 3.13 The measurement schematic of LDV

The gas-phase flows, at the center and off-center of the x-axis, were measured by the LDV system. Figure 3.13 is the schematic setup of the LDV measurements. The experimental results had good reproducibility ($<5\%$ error). The following discussion focuses on the two measurement regions shown in Figure 3.13. Positions in region II were measured to figure out the influence of flame spread on the surrounding air. The gas-phase flow in region I was heavily investigated to study the flow pattern and behavior of the flame spread.

3.3.2 Gas phase Velocity along the tray centerline

The VEL(1), VEL(2) and VEL(3) on the graphs in Figures 3.14-3.17 are three velocity components in the directions of x, y and z respectively. The velocity unit on the graphs is meter per second (m/s). Experiments were conducted at an initial pool temperature of 19°C with propanol. The initial pool temperature range of pulsating flame spread for propanol was 14-23°C.

Figure 3.14 gives the transient velocity map of the gas-phase at the position $x=0$ and $y=0$. Before the flame front reached the measurement point, the velocity of gas fluctuated at 0.01 m/s. After the flame front passed the measurement point, the upward velocity (VEL(3), direction z) component increased from 0.01 m/s to 1 m/s at $z=120$ mm. Right ahead of the flame, the velocities VEL(1) (x-direction) and VEL(2)) (y-direction) at $z=5$ mm (Figure 3.14.a) increased from 0.01 m/s to -0.1 m/s and $+0.1$ m/s respectively. Thus, there was a tenfold increase in the gas flow towards and from the side of the flame. In addition, VEL(3) showed that a very slow air flow moved from the top towards the flame. At $z=40$ mm, the velocity of airflow in the x direction (VEL(1)) increased and the flow direction reversed, suggesting the existence of a vortex. Side flow toward the flame and upward airflow became stronger than at $z=5$ mm. At $z=80$ mm and 120 mm, upward flow was still very strong (up to 1 m/s) and unstable flows in the x and y directions were observed. The 3-D LDV data in Figure 3.14 supported the PIV and HSVS investigation regarding the flow directions. The results for the LDV, PIV, and HSVS methods, even for the unstable flows, were reproducible based on image comparisons and standard error calculations.

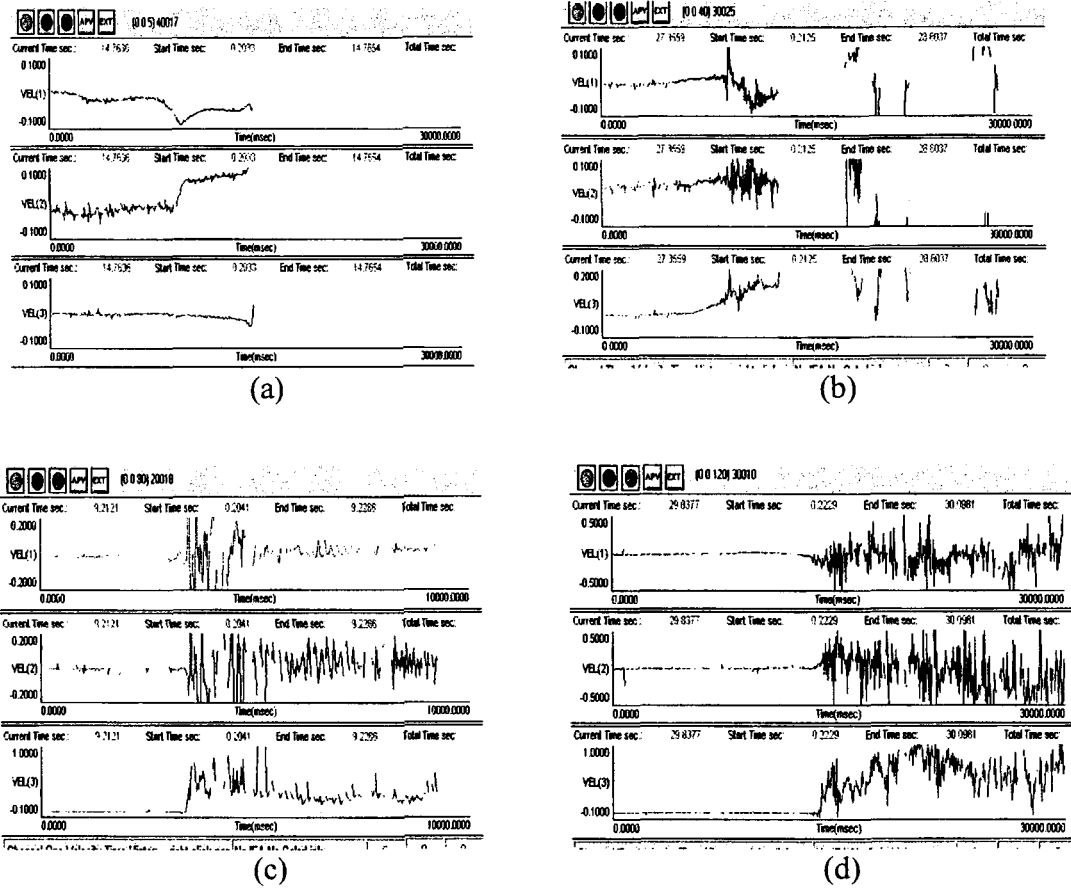


Figure 3.14 LDV Velocity components above the liquid surface at $x=0, y=0$

(a) $z=5$ mm (b) $z=40$ mm (c) $z=80$ mm (d) $z=120$ mm

3.3.3 Gas phase velocity off the tray centerline

Figure 3.15 shows velocity components off the center of the pool at 5 mm above the liquid surface. According to these three figures and referring to Figure 3.14, we can conclude that: 1) before the flame front reached the measurement point, the velocity of gas at these points fluctuated at 0.01 m/s level. 2) The flame spread had little influence on the upward velocity (VEL(3), direction z) component at these measured positions. 3) VEL(1), (the direction of flame spread, i.e. direction x) reduced to approximate -0.1 m/s in all cases when the flame front reached the measurement point and then reversed

direction. That means the gas flow and flame spread near the flame front reversed direction with the gas movement towards the flame. The figures show that VEL(2) (side direction, i.e., direction y) was in the direction towards the flame center from the surroundings.

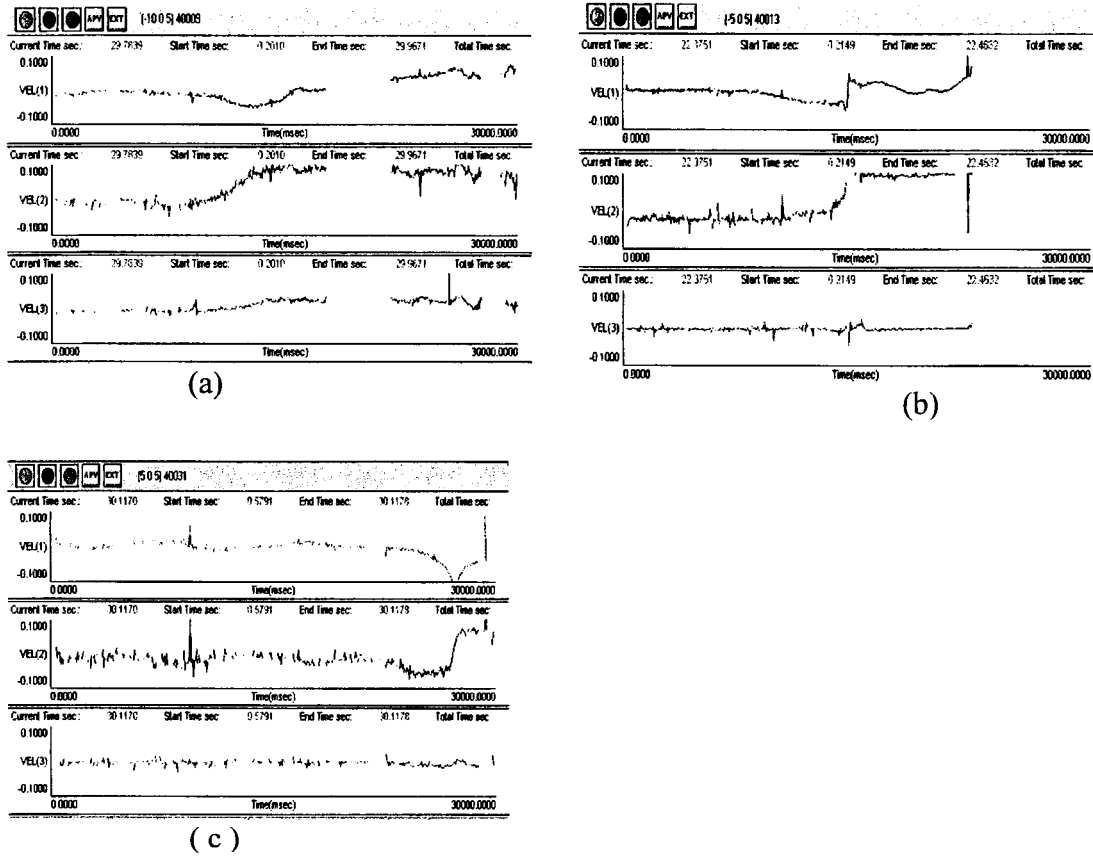


Figure 3.15 LDV velocity components off the flame center and at Z=5 mm.

(a) $y=-10$ mm, (b) $y=-5$ mm, (c) $y=5$ mm

Figure 3.16 is the flow velocity of the gas-phase outside the flame at 80 mm above the pool and 40 mm off the flame center. It shows the influence of the flame spread on the gas phase surrounding. According to Figure 3.16, VEL(1) was in the direction against/opposite the flame at the measured point and VEL(2) was in the direction into the flame from the surrounding with VEL(3) fluctuating around zero.

Figures 3.16 and Figure 3.14 (c) also show that the fluctuations in the velocities were reduced after the flame front passed the measurement point.

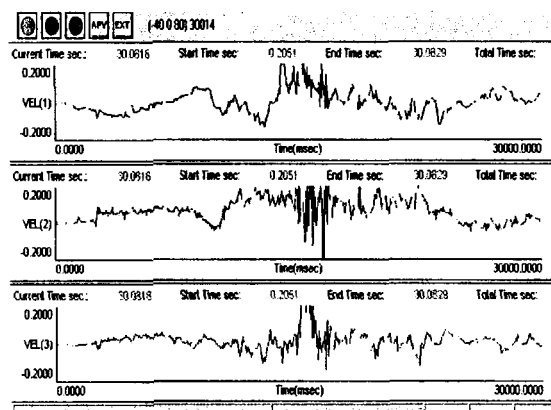


Figure 3.16 Flow velocity of gas-phase off the flame center by 40 mm

Figure 3.17 is the velocity at 80 mm above the pool and at the centerline of the flame. It shows that after passage of the flame, the z component of the velocity, VEL(3), was significantly higher at the centerline than 40 mm off center. The x and y velocity components, VEL(1) and VEL(2), had wider fluctuation around 0 m/s for the centerline case.

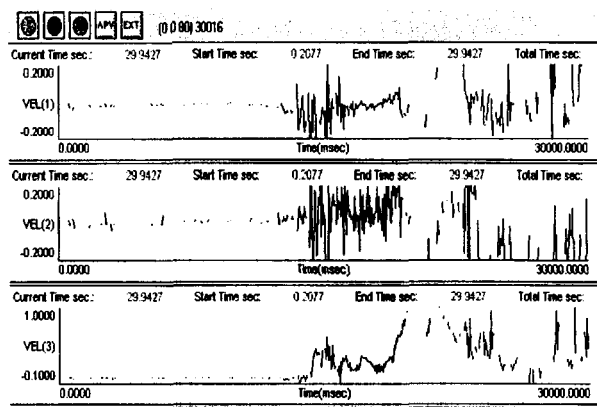


Figure 3.17 Flow velocity of gas-phase at the centerline of the flame

3.3.4 Summary discussion on LDV experiments

Fig.3.18 is a schematic representation of the gas flow pattern ahead of and close to the flame front based on the LDV measurements. The influence of flame spread on the upward velocity (i.e. VEL(3)) increased with increase of height of measurement point above the pool within the measurement range (<80 cm), but reduced sharply with increase of the distance in the y direction between the measurement point and flame, which shows that buoyancy is the major driving force for the gas upward movement.

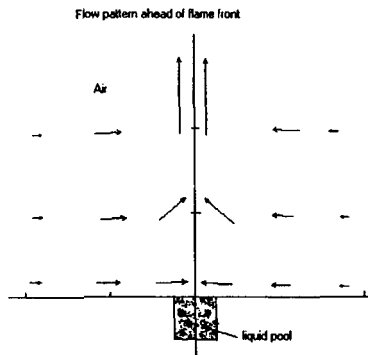


Figure 3.18 The schematic gas flow pattern ahead of and close to the flame front

The air flow towards the flame ahead of the flame front reversed direction just before the flame front, suggesting the creation or existence of a vortex ahead of the flame front. The existence of the vortex was confirmed by the PIV and HSVS system as discussed earlier.

The instability of flow inside the flame reached a maximum within a short time after the flame front passed and then went back to a relative steady behavior, which was also observed by the PIV and High Speed Video System in our earlier investigation. The observation indicates that the maximum turbulence occurs near the flame front.

3.4 LDV Candle Analysis

LDV measurements around a candle flame were conducted to investigate the flow pattern and the influence of buoyancy on the candle flame.

3.4.1 The experimental setup

The major components of the experimental setup and instrumentation for the candle flame analysis included LDV system, a transparent Plexiglas box with a vent hole on the top cover, an experimental table, a smoke generator, and candles.

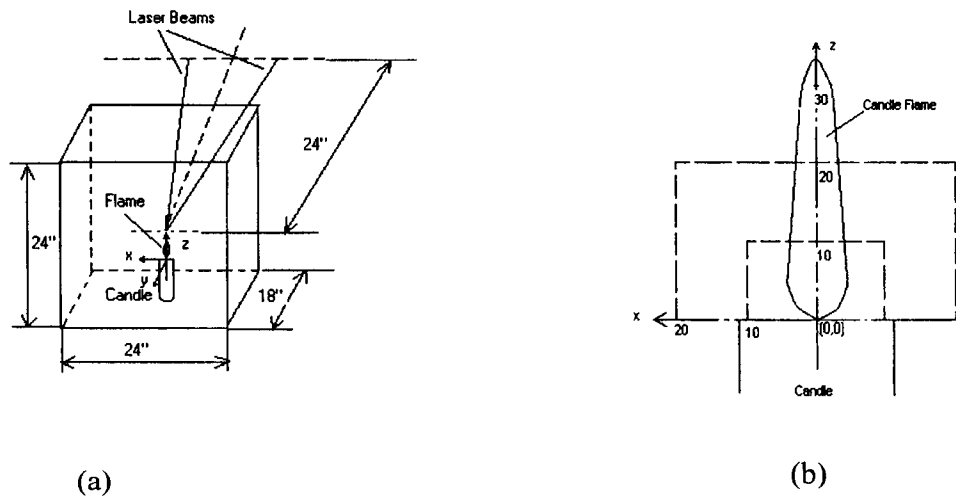


Figure 3.19 Measurement schematic of candle flame experiment

Figure 3.19 is the schematic of the experimental setup for the candle flame investigation. The candle was fixed at the center of a transparent Plexiglas box to make the flame axisymmetric. The Plexiglas box ensured a quiescent environment. The size of this box was 61 cm in width and length and 46 cm in height. The laser beams were transmitted from the probes of the LDV system. The probes were fixed on a traverse system, capable of changing measurement positions in 3-dimensions. Figure 3.20 is a

photograph of the experimental setup with the LDV system. The smoke generator was used for seeding in these experiments.

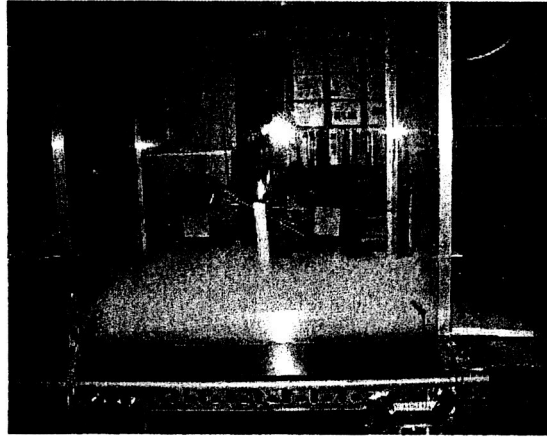


Figure 3.20 Photo of experimental setup

Experimental investigations were conducted at a fixed condition. It was a quiescent Plexiglas enclosure with a top cover and a small vent. The room temperature was about 23°C. The measurements were focused on the lower and nearby region of the candle flame as shown in Figure 3.19 (b) (The larger enclosure region). Two candles were used for the experiments. One candle had a radius of 11 mm and was labeled R11 and another with radius of 20 mm was labeled R20. Their cords were approximate 1.5 mm. In the experiments, it was assumed that the flame and the flow were symmetrical to the z axis and were at steady state.

3.4.2 The experiments with candle R11

Figure 3.21 gives the measurement position plan with candle R11. The measurements start from $z=20$ mm, $x=-18$ mm. First, $z=20$ mm was fixed and x was changed from $x=-18$ mm to $x=0$ with step increases of 1 mm or 2 mm. The values of z were reduced from $z=20$ mm to $z=-6$ mm at 2 mm intervals and at each fixed z the values

of x were changed as above, from $x = -18$ mm to 0 mm by step increase of 1 mm or 2 mm, for the measurements. The candle cord was set in the z axis and the top of the candle (i.e. base of the flame) was set on the x - y plane as shown in Figure 3.1 (b). The blank area or region without data points is where valid velocity data could not be obtained because the seeding particles could not reach or distribute evenly in the region.

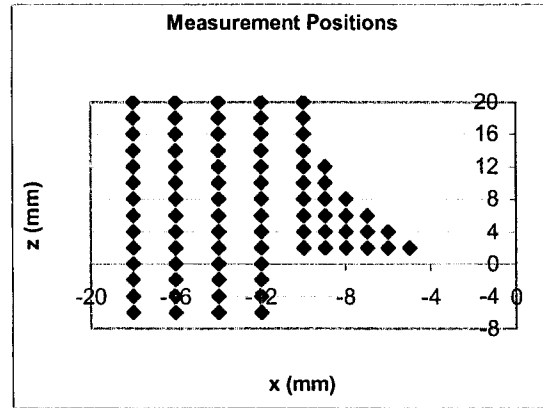


Figure 3.21 Measurement Positions with (R11)

Figures 3.22 to 3.25 are the velocity distributions at different positions and with different candles. In the figures, U_x expresses the radial component of the measured flow, U_z expresses its axial component and U_y is supposed to be noise due to the axisymmetrical nature of the flow.

Figure 3.22 shows that the noise velocity U_y fluctuates between ± 10 mm/s, which means the noise is at a level of 10 mm/s. The radial velocity components are always positive (toward the candle center) and between 30 mm/s and 50 mm/s. The axis velocity components are positive (upward) and vary significantly along with the change of x , the distance between the measurement position and the flame. The closer to the flame the measurement position, the faster the upward velocity component increased. It

increased from 0 up to 100 mm/s when z changed from 2 mm to 12 mm, with $x=-6 \sim -10$ mm, due to buoyancy.

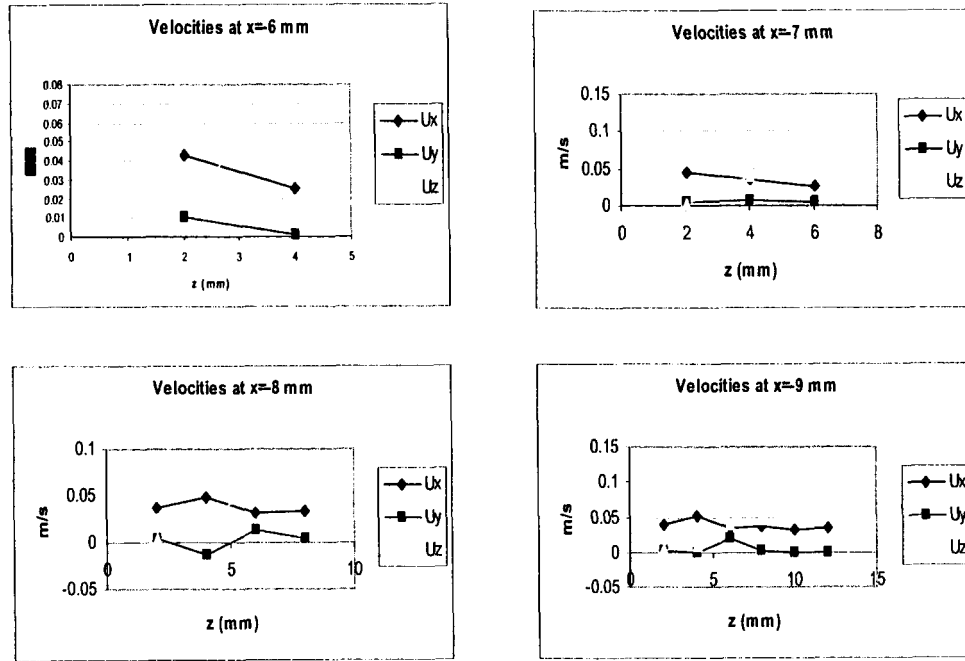


Figure 3.22 The velocity distribution (R11, $x=-6 \sim -9$ mm)

Figure 3.23 shows that around $x=-12$ mm and $z=0$ mm, more fluctuations (velocity components in directions x and y) can be seen in the flow due to the larger ratio (about 0.5) of the flame diameter to the candle diameter. The figure also shows that the upward velocities and their fluctuations below $z=0$ are higher than those above $z=0$ within the interest area.

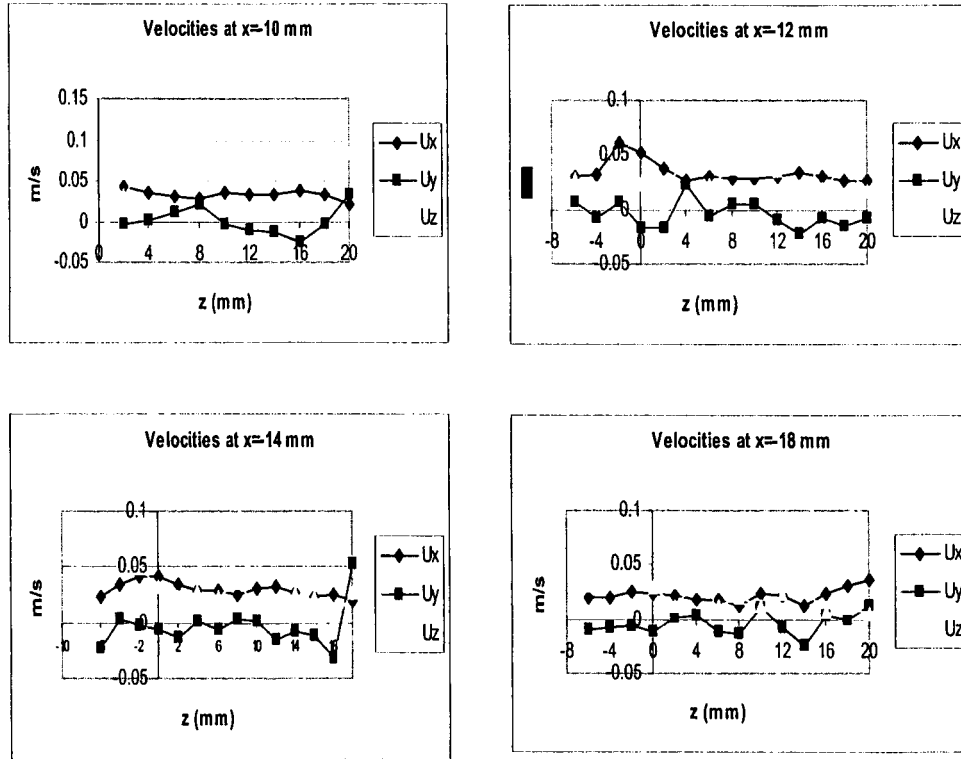


Figure 3.23 The velocity distribution (R11, $x=-10\sim-18$ mm)

3.4.3 The experiments with candle R20

Figure 3.24 is the measurement position arrangement with candle R20. It is similar to that for R11 candle. The measurements started from $z=20$ mm, $x=-20$ mm. First, $z=20$ mm was fixed and x was changed from -20 mm to 0 mm with step increases of 2 mm. The z values were then decreased at intervals of 2 mm until $z=0$. At each fixed z , the values of x were changed from $x=-20$ mm to 0 mm with step increases of 2 mm. The candle cord was set in the z axis and the top of the candle (i.e., base of the flame) was set in the x - y plane as shown in Figure 3.19 (b). The blank area near the flame is the

region where valid velocity data could not be obtained due to seeding problems as explained earlier.

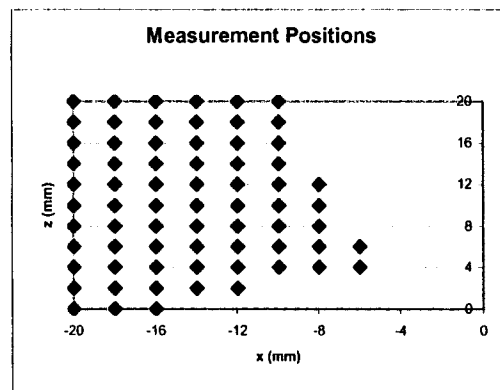


Figure 3.24 Measurement positions with (R20)

Figure 3.25 also showed similar characteristics as Figures 3.22 and Figure 3.23. Its characteristics are consistent through the entire measured region. It did not show the flow fluctuations around $x = -12$ mm and $z = 0$ because this solid candle had a much smaller ratio of flame to candle diameter. Besides, it showed more clearly than Figures 3.22 and 3.23 that the radial components decreased with the increase of the distance from the measurement point to the flame and the axial upward components increased with the increase of the height of the measurement position.

The results of the experiments with different candle radii suggests that the candle radius used in the experiments does not strongly affect the flow pattern around the candle flame.

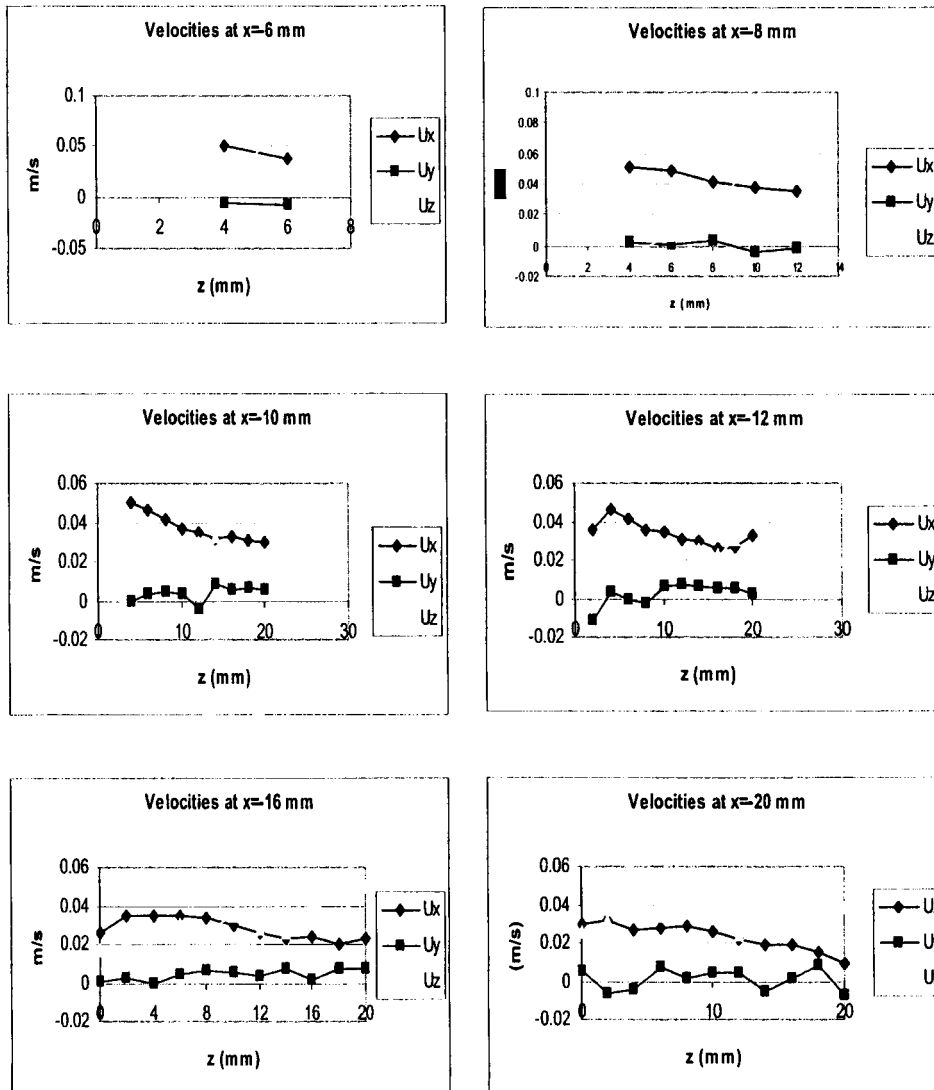


Figure 3.25 The velocity distribution (R20, $x=-6\sim 20$ mm)

3.4.4 Discussion of the experimental results

Figure 3.26 is the PIV image of the flow field around the candle flame. It shows the visual flow field at the measurement region of the candle flame.



Figure 3.26 The PIV image of candle flow field

The velocity profile for the candle flame in the measured region can be seen in Figure 3.27. At the nearby region (within 20 mm radius from the flame center), the direction of radial components was always toward the candle center and the direction of axial components was upwards. The magnitudes of the radial components did not change significantly. However, the upward components sharply changed. The closer to the flame the measurement position, the faster the upward components increased.

The experiments also showed that the fluctuation in the y component velocity increased with increasing distance from the flame, especially, at 12 mm away from the flame center, within the measurement region. These characteristics suggest that the temperature and mass gradients control the flow within 10 mm of the flame center and the influence of the flame is reduced significantly between 10 mm and 20 mm to the flame center.

From the experiments, there was no noticeable vortex found in the measurement region under the test conditions.

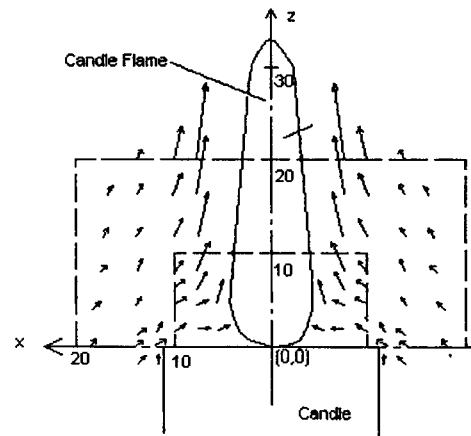


Figure 3.27 The flow patten of the candle flame

4. SUMMARY AND CONCLUSIONS

1. Three regimes of flame spread behavior were experimentally investigated and the flame position vs. time graphs were obtained through PIV and high-speed images. In the pulsating regime, the jump velocity appeared to be independent of initial pool temperature. However, the crawl velocity was dependent on initial pool temperature. The velocity vector distribution in the liquid phase was obtained by PIV system. The size of the transient subsurface vortex in the liquid phase below the flame front decreased as the initial pool temperature increased.
2. A vortex within 5 mm above the gas-liquid interface was clearly observed in the gas phase just ahead of the flame front in the propagation direction through the PIV images. The size of the vortex in the gas phase ahead of the flame front decreased as the initial pool temperature increased. This experimental finding confirmed the existence of the vortex predicted by numerical analysis [14]. We found vortices in all three flame spread regimes in the liquid phase. However, we did not obtain them in the gas phase at the uniform and pulsating regimes at higher initial pool temperatures.
3. The flow near the liquid-gas interface and the vortex below the flame front played an important role in the formation and the size of the vortex in the gas phase. After reaching a maximum, the liquid flow velocity below the flame front started to reduce sharply, which led to the change of the previous thin laminar flow at the interface that might have induced a gas phase vortex. It is believed that the velocity changes significantly contribute to the formation of the vortex in the gas phase ahead of the flame front because the changes affect fuel evaporation, thermal gradients in the

liquid, and convection although it is not clear which of the flow driving forces directly determine the formation of the vortex. The vortex in the gas phase was very small and became smaller as the initial pool temperature increased. The dependence of the vortex size on the initial pool temperature may explain why the vortex in the gas phase was not observed in the pulsating regime at higher initial pool temperatures.

4. Two gas phase vortices existed over the liquid surface, according to the test results from the side view. The higher the initial pool temperature, the more gasified fuel and the larger the two recirculation cells and the triangular premixed zone. Buoyancy of the gasified fuel over the tray was believed to be one of the important contributing factors of the characteristics of the premixed zone.
5. A tentative explanation to the formation of pulsating behavior of flame spread is presented. When the interface flow is faster than the flame spread (pseudo-uniform regime), thermal expansion of the flame is slow to reach the vortex ahead of the flame front; when the flame spread is much faster than the interface flow (uniform regime), thermal expansion of the flame breaks the vortex before it is really formed. When the flame spread velocity and interface flow rate are comparable (pulsating regime), thermal expansion can reach and break or destroy the gas phase vortex ahead of the flame front. Once broken and during the crawl period, the fuel accumulates until an ignitable mixture is formed and the flame advances again with a jump. This may explain the observation of the pulsating behavior which is consistent with previous numerical analysis [14].

6. LDV measurements around candle flames were also conducted to investigate the flow pattern and the influence of buoyancy on the candle flame. At the nearby region (within 20 mm radius from the flame center) the direction of radial components was always toward the candle center and the direction of axial components was upwards. The magnitudes of the radial components did not change significantly. However, the upward components dramatically changed. The closer to the flame the measurement position, the faster the upward components increased. The experiments also showed that the fluctuations in velocities increased with increasing distance from the flame, especially, at 12 mm away from the flame center. These characteristics suggested that the temperature and mass gradients control the flow within 10 mm from the flame center and the influence of the flame is reduced significantly between 10 mm and 20 mm off the flame center. There was no noticeable vortex found in the measured regions under the test conditions.

5. RECOMMENDATIONS

Further work on the fire spread behavior in liquid pools is suggested to include the determination of the role of thermal expansion and gas-phase buoyancy, the measurements of velocities off the tray axis in the liquid phase below the surface under high temperature and pressure conditions, and the quantification of the effects of force flow on fire behaviors in normal gravity.

The candle work also needs to be expanded to provide more insight into the flow structure and field around the burning candle.

REFERENCES

1. Kinbara, T., Surface Combustion Phenomena of Liquids, Rikagaku-Kenkyusho Shuho, Bull. Inst. Phys. Chem. Research, Tokyo, 1931
2. Glassman, I. And Dryer, F., Fire Safety J., 3,132, 1981
3. Ross, H.D, Ignition of and Flame Spread Over Laboratory-scale Pools of Pure Liquid Fuels, Prog. Energy Combust. Sci. , vol 20, pp17-63, 1994.
4. Ross, H. D. and F. Miller, "Flame spread across liquid pools," Chapter 5 in Microgravity Combustion, ed. Howard D. Ross, Academic Press, San Diego, 2001
5. Ito, A., Masuda, D. and Saito, K. (1991). "A Study of Flame Spread Over Alcohols with Holographic Interferometry." Combustion and Flame 83: 375-389.
6. Miller, F. J. and H. D. Ross (1995). Liquid-Phase Velocity and Temperature Fields During Uniform Flame Spread Over 1-Propanol. 8th International Symposium on Transport Processor in Combustion. San Francisco, CA. July, 1995.
7. Newman, J., MSE Thesis, Dept. of Mech. and Aerospace Eng., Princeton Univ. Princeton, NJ 1979.
8. Santoro, R. J., Fernandez-Pello, A. C., Dryer, F. L., and Glassman, I., *App. Optics*, 17, 3843, 1, (1978).
9. Garcia-Ybarra, P. L. e. a. (1996). Study of Thermocapillary Layer Proceeding Slow, Steadily Spreading Flames over Liquid Fuels. 26th International Symposium on Combustion, Naples, Italy, The Combustion Institute.
10. Furuta, M., Humphrey, J. A. C., Fernandez-Pello, A. C., *Physico. Chem. Hydrodyn.*, 6, 347 (1985).of Velocity and Fuel Concentration over Liquids." ASME Heat Transfer Division HTD-Vol. 352: 141-148.
11. Sirignano, W. A., Combust. Sci. Technol., 6:95 (1972)
12. Miller, F. J. a. R., H. D. (1998). Smoke Visualization of the Gas-Phase Flow During Flame Spread Across a Liquid Pool. 27th International Symposium on Combustion, Boulder, Colorado, The Combustion Institute.
13. Ito, A., Narumi, A., Konoshi, T., Tashtoush, G., Saito, K., and Cramers, C. J. (1997). "The Measurement of Transient 2-D Profiles of Velocity and Fuel Concentration over Liquids." ASME Heat Transfer Division HTD-Vol. 352: 141-148.
14. Schiller, D.N., Ross, H.D., Sirignano, W.A., "Computational Analysis of Flame Spread Across Alcohol Pools," Combustion Science and Technology, vol.118, no.4-6, pp.203+/1996.